Dear author,

Please note that changes made in the online proofing system will be added to the article before publication but are not reflected in this PDF.

We also ask that this file not be used for submitting corrections.

International Journal of Solids and Structures xxx (xxxx) xxx

Contents lists available at ScienceDirect

International Journal of Solids and Structures

journal homepage: www.elsevier.com/locate/ijsolstr

Effect of pair coalescence of circular pores on the overall elastic properties

Q1 L. Lanzoni[a], E. Radi[b], I. Sevostianov[c,*]

[a] Dipartimento di Ingegneria "Enzo Ferrari", Università di Modena e Reggio Emilia, Via Vivarelli, 10 41125 Modena, Italy
[b] Dipartimento di Scienze e Metodi dell'Ingegneria, Università di Modena e Reggio Emilia, Via Amendola, 2 42122 Reggio Emilia, Italy
[c] Department of Mechanical and Aerospace Engineering, New Mexico State University, Las Cruces, NM 88001, USA

ARTICLE INFO

Article history:
Received 28 February 2019
Revised 14 May 2019
Accepted 14 May 2019
Available online xxx

Keywords:
Cylindrical pores
Irregular cross-section
Bipolar coordinates
Compliance contribution tensor
Effective elastic

ABSTRACT

The paper focuses on the effect of the pair coalescence of circular pores on the overall elastic properties. An analytic solution for the stress and displacement fields in an infinite elastic medium, containing cylindrical pore with the cross-section formed by two circles, and subjected to remotely applied uniform stresses is obtained. The displacement field on the surface of the pore is then determined as a function of the geometrical parameters. This result is used to calculate compliance contribution tensor for the pore and to evaluate effective elastic properties of a material containing multiple pores of such a shape.

1. Introduction

In the present paper we focus on the effect of the pair coalescence of circular pores on the overall elastic properties. The research is motivated mostly be needs to predict properties of porous materials obtained by Gasar technology – process consisting of a melting metal in a gas atmosphere to saturate it with hydrogen and directional solidification (Shapovalov, 1994; Shapovalov and Boyko, 2004). The pores have cylindrical shape and are nucleated heterogeneously. The process is accompanied by pores coalescence. Shapovlov (1998) showed that the pore coalescence becomes prominent for Gasar metals with high porosity. The modeling of the evolution process of pore coalescence has been proposed by Liu et al. (2018). Fig. 1 illustrates the process of the pores coalescence and the resulting shapes of the pores' cross-sections in Gasar metals.

We consider this material in the framework of plane-strain problem and assume that it contains aligned cylindrical inhomogeneities of certain cross-sectional shape. Analytical modeling of materials with inhomogeneities of non-elliptical cross-section is not well developed though many two-dimensional problems have been solved. The main approaches to this problem are:

- Complex variables technique involving conformal mapping of the cross-sectional shape onto a unit circle (Kachanov et al., 1994). For many non-elliptical shapes, the transformation

$$z(\zeta) = R\left(\frac{1}{\zeta} + \sum_{n=1}^{N} a_n \zeta^n\right) \tag{1.1}$$

that maps conformally the exterior of the inhomogeneity in the complex z-plane into the interior of a unit circle in the ζ-plane, is used, with parameters R, N and a_n corresponding to various shapes; for the elliptical hole, for example, $N = 1$, $R = (a + b)/2$ and $a_1 = (a - b)/(a + b)$. For "irregular" shapes, a numerical mapping technique can be used (see Tsukrov and Novak, 2004);

- Finite element method, that is more universal, applies to inhomogeneities of arbitrary elastic properties, including anisotropic ones, but has lower accuracy than the numerical conformal mapping technique. Comparison of the two methods was given by Tsukrov and Novak (2002).

Compressibility of non-elliptical holes has been first analyzed by Zimmerman (1986) on the example of super-circular holes (convex and concave), by Givoli and Elishakoff (1992) and Ekneligoda and Zimmerman (2008a) who considered holes with "corrugated" boundaries and by Ekneligoda and Zimmerman (2006, 2008b) who considered shapes having n-fold symmetry axes. Results for the entire compliance contribution tensor of a non-elliptical hole have been obtained by

* Corresponding author.
E-mail address: igor@nmsu.edu (I. Sevostianov).

https://doi.org/10.1016/j.ijsolstr.2019.05.012

Please cite this article as: L. Lanzoni, E. Radi and I. Sevostianov, Effect of pair coalescence of circular pores on the overall elastic properties, International Journal of Solids and Structures, https://doi.org/10.1016/j.ijsolstr.2019.05.012

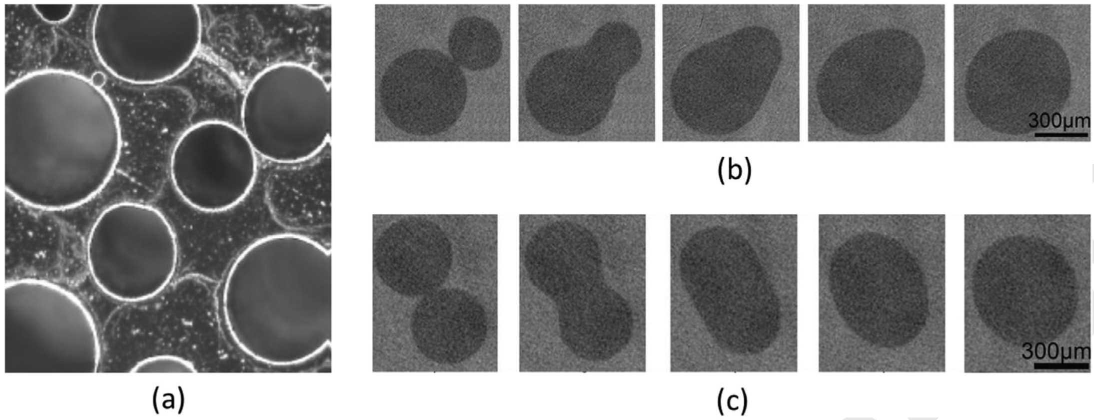

Fig. 1. (a) Pores structure in Gasar Ni-15%Al, intermetallic compound (shape of pores is almost cylindrical, from Drenchev and Sobczak, 2009); (b) and (c) evolution of two pores coalescence in Gasar copper (from Liu et al., 2018).

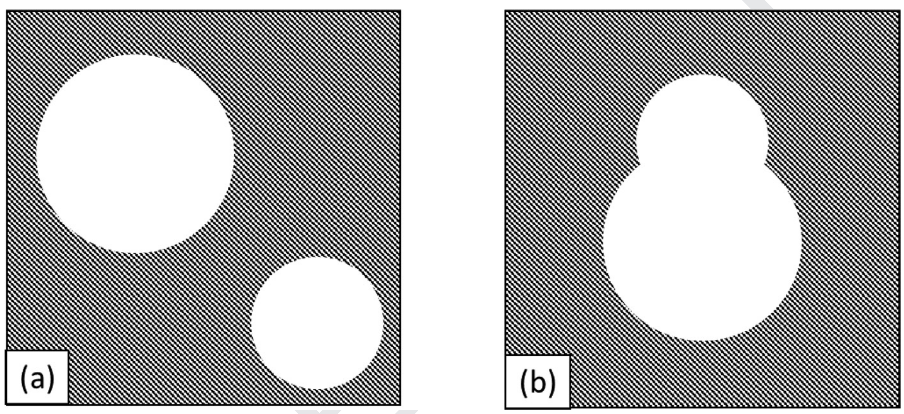

Fig. 2. (a) two separate circular holes, (b) cross-section formed by two coalesced circular pores of generally different radii.

Kachanov et al. (1994) and Jasiuk (1995) for various polygons (convex and concave) and Tsukrov and Novak (2002, 2004) for several “irregular” shapes.

The present paper continues authors’ work (Lanzoni et al., 2018) on the shapes that may be obtained by union of two circles of generally different diameters (Fig. 2). We consider isotropic elastic plane containing two circular holes of radii r_1 and r_2 (that may overlap). Thus, the pore shapes may be non-convex and even not simply connected. Instead of the conformal mapping technique (that may be a problem in this case since connectivity of the pore may change) we use an analytic approach based on Fourier series representation or Fourier transform in bipolar coordinates (Jeffery, 1921), $(\alpha,\ \beta)$ (Fig. 3), related to the Cartesian coordinates (x_1,x_2) by

$$\alpha = \mathrm{Re}\left[\ln\frac{(x_1+ix_2)+a}{(x_1+ix_2)-a}\right]; \qquad \beta = -\mathrm{Im}\left[\ln\frac{(x_1+ix_2)+a}{(x_1+ix_2)-a}\right]; \tag{1.2}$$

$$x_1 = \frac{a\sinh\alpha}{\cosh\alpha-\cos\beta}; \qquad x_2 = \frac{a\sin\beta}{\cosh\alpha-\cos\beta}. \tag{1.3}$$

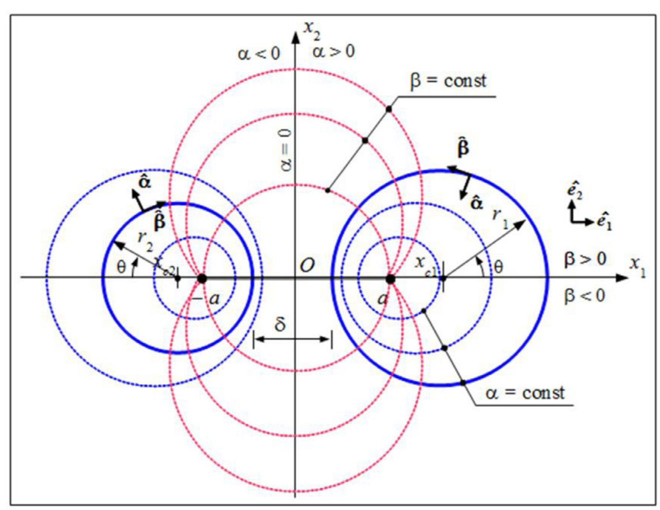

Fig. 3. Sketch of the bipolar coordinate system.

Note, that β-coordinate is multi-valued with a discontinuity of 2π across the segment connecting the foci. Hereinafter, we assume $-\pi < \beta \le \pi$. The two poles of the bipolar coordinates are located on the x_1 axis at distance $\pm\, a$, with $a > 0$ (the circles in Fig. 2(a) refers to $\alpha_1 > 0$ and $\alpha_2 < 0$ whereas Fig. 2(b) shows two overlapping circles with $\beta_1 > 0$ and $\beta_2 < 0$).

First, we consider a single inhomogeneity and solve Neumann boundary value problem in two-steps: (1) assessment of the fundamental displacement field related to a remotely applied uniform stress in a homogeneous body and (2) fulfillment of the boundary conditions by adding an extra-term to the fundamental field. This solution is used to construct the compliance contribution tensor of a pore of interest by calculating proper contour integrals. The compliance contribution tensor can be used to calculate overall elastic properties of a material containing parallel cylindrical holes with the cross-sections shown in Fig. 2.

Please cite this article as: L. Lanzoni, E. Radi and I. Sevostianov, Effect of pair coalescence of circular pores on the overall elastic properties, International Journal of Solids and Structures, https://doi.org/10.1016/j.ijsolstr.2019.05.012

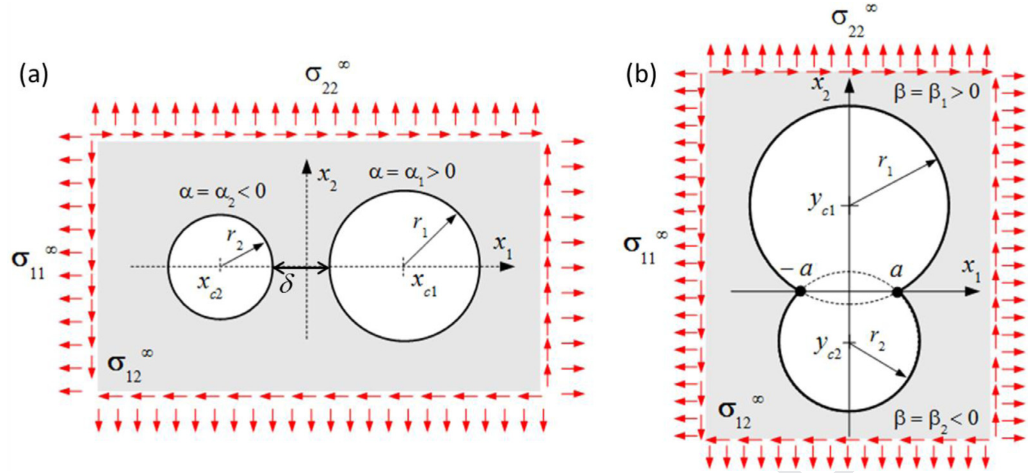

Fig. 4. Sketch of an infinite plate with (a) two separate holes and (b) two merging holes subjected to remote normal $\sigma^{\infty}{}_{11}$, $\sigma^{\infty}{}_{22}$ and shear $\sigma^{\infty}{}_{12}$ stress fields along the principal directions x_1, x_2.

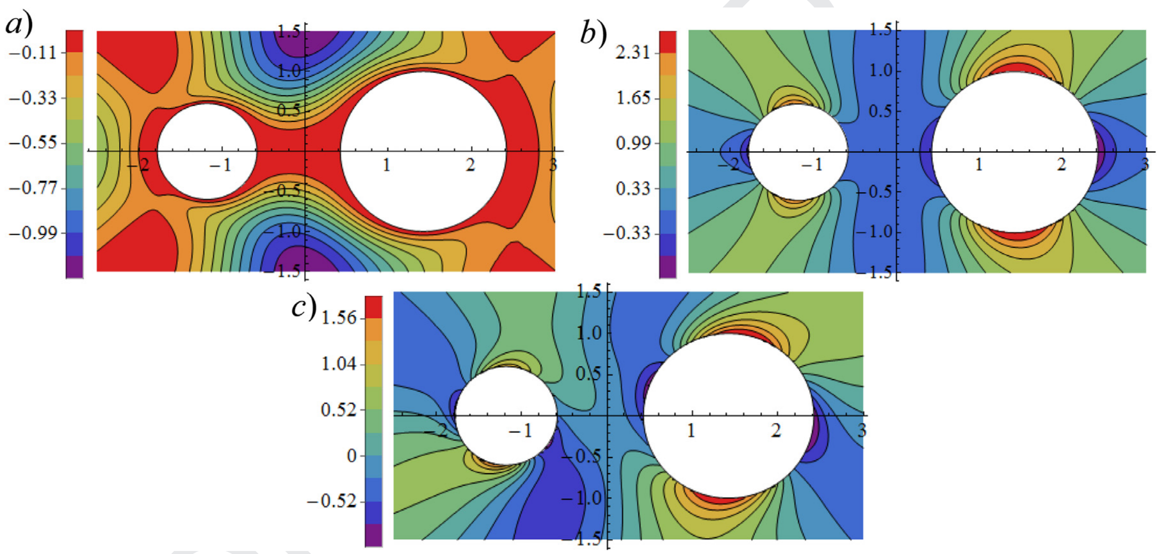

Fig. 5. Distribution of the dimensionless stress fields (a) $\sigma_{\alpha\alpha}/\sigma^{\infty}{}_{11}$; (b) $\sigma_{\beta\beta}/\sigma^{\infty}{}_{11}$; (c) $\sigma_{\alpha\beta}/\sigma^{\infty}{}_{11}$ in a plate subjected to a remote stress in the x_1 direction for $\rho=3/5$, $\gamma=1$.

2. Two separate circular holes

In this Section we briefly summarize the known results about elastic fields in an infinite plate containing two separate circular holes of radii r_1 and r_2 in an infinite plane separated by the ligament δ between them. For the case of two holes of the same radius the problem was solved by Ling (1947, 1948a) for remotely applied normal loadings and by Karunes (1953) for remotely applied shear loading. Radi (2011) generalized their solutions for two holes of different radii.

The geometry of the problem is completely determined by two independent geometrical parameters: for example, ratio of the radii $\rho\equiv r_1/r_2$ and relative length of the ligament $\gamma\equiv\delta/r_1$ (Fig. 4):

$$\begin{aligned}&x_{c1}=r_1+\delta[1-(r_1+0.5\delta)/(r_1+r_2+\delta)];\\&\alpha_1=\operatorname{arccos}h\,(x_{c1}/r_1);\quad a=r_1\sinh(\alpha_1);\\&\alpha_2=-\operatorname{arcsin}h(a/r_2);\quad x_{c2}=-r_2\cosh\alpha_2.\end{aligned}\tag{2.1}$$

The plane is subjected to the action of remotely applied stresses σ_{11}^{∞}, σ_{22}^{∞}, and σ_{12}^{∞}.

The traction free boundary conditions

$$\sigma_\alpha=\tau_{\alpha\beta}=0 \text{ for } \alpha=\alpha_1,\ \alpha_2\tag{2.2}$$

have to be satisfied at the holes.

The stress field, corresponding to the biharmonic Airy stress function χ is given by Jeffery (1921):

$$\begin{aligned}\sigma_\alpha&=-\left[(\cosh\alpha-\cos\beta)\frac{\partial^2}{\partial\beta^2}-\sinh\alpha\frac{\partial}{\partial\alpha}-\sin\beta\frac{\partial}{\partial\beta}+\cosh\alpha\right]h_\chi;\\\sigma_\beta&=-\left[(\cosh\alpha-\cos\beta)\frac{\partial^2}{\partial\alpha^2}-\sinh\alpha\frac{\partial}{\partial\alpha}-\sin\beta\frac{\partial}{\partial\beta}+\cos\beta\right]h_\chi;\\\tau_{\alpha\beta}&=(\cosh\alpha-\cos\beta)\frac{\partial^2 h_\chi}{\partial\beta\partial\alpha},\end{aligned}\tag{2.4}$$

where

$$h_\chi=\frac{\chi}{a}(\cosh\alpha-\cos\beta).\tag{2.5}$$

The Airy function χ can be represented as the sum of a fundamental stress function $\chi^{(0)}$, which gives the uniform stresses applied at infinity but does not yield vanishing tractions on the circular boundaries, and an auxiliary stress function $\chi^{(1)}$, required to satisfy the boundary conditions (2.2), which gives zero stresses at infinity. Correspondingly,

$$h_\chi=h_\chi^{(0)}+h_\chi^{(1)},\tag{2.6}$$

Please cite this article as: L. Lanzoni, E. Radi and I. Sevostianov, Effect of pair coalescence of circular pores on the overall elastic properties, International Journal of Solids and Structures, https://doi.org/10.1016/j.ijsolstr.2019.05.012

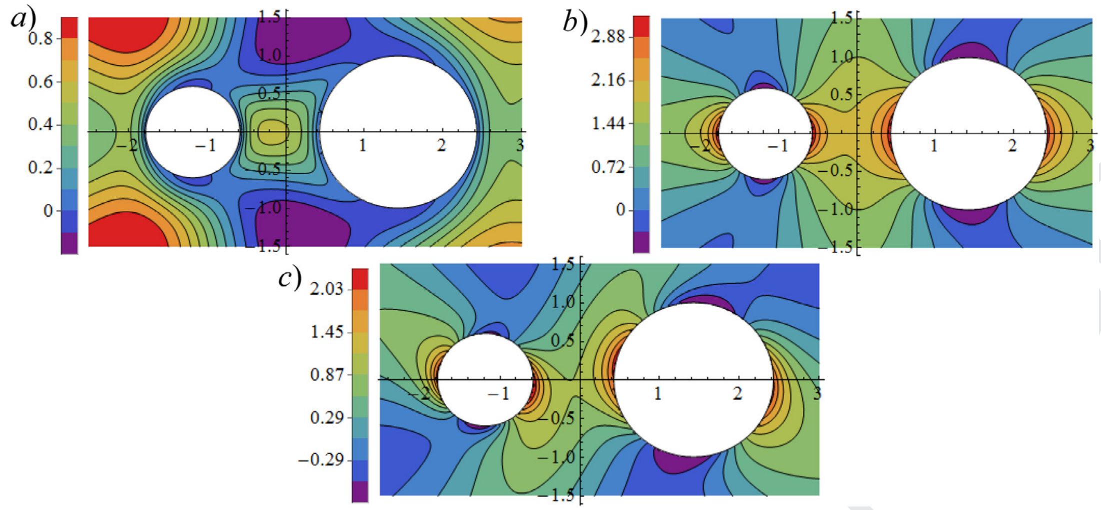

Fig. 6. Distribution of the dimensionless stress fields (a) $\sigma_{\alpha\alpha}/\sigma^{\infty}{}_{22}$; (b) $\sigma_{\beta\beta}/\sigma^{\infty}{}_{22}$; (c) $\sigma_{\alpha\beta}/\sigma^{\infty}{}_{22}$ in a plate subjected to a remote stress in the x_2 direction for $\rho = 3/5$, $\gamma = 1$.

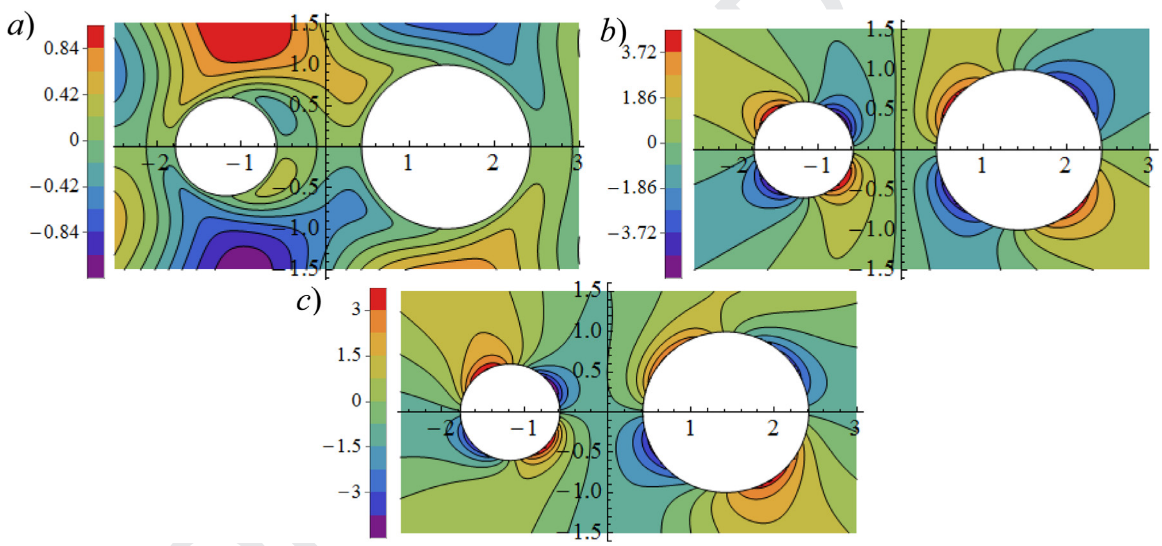

Fig. 7. Distribution of the dimensionless stress fields (a) $\sigma_{\alpha\alpha}/\sigma^{\infty}{}_{12}$; (b) $\sigma_{\beta\beta}/\sigma^{\infty}{}_{12}$; (c) $\sigma_{\alpha\beta}/\sigma^{\infty}{}_{12}$ in a plate subjected to a remote shear stress in the $x_1 x_2$ plane for $\rho = 3/5$, $\gamma = 1$.

where

$$h_\chi^{(0)} = \frac{(\sigma_{11}^\infty \sin^2\beta + \sigma_{22}^\infty \sinh^2\alpha - 2\sigma_{12}^\infty \sin\beta \sinh\alpha)}{2(\cosh\alpha - \cos\beta)}. \tag{2.7}$$

$$h_\chi^{(1)} = [B\alpha + K \ln(\cosh\alpha - \cos\beta)](\cosh\alpha - \cos\beta) + \sum_{n=1}^{\infty} \phi_n(\alpha)\cos n\beta + \psi_n(\alpha)\sin n\beta. \tag{2.8}$$

Functions $\varphi_n(\alpha)$ and $\psi_n(\alpha)$ are given by

$$\begin{aligned} \phi_n(\alpha) &= A_n \cosh(n+1)\alpha + B_n \cosh(n-1)\alpha \\ &\quad + C_n \sinh(n+1)\alpha + D_n \sinh(n-1)\alpha; \\ \psi_n(\alpha) &= a_n \cosh(n+1)\alpha + b_n \cosh(n-1)\alpha \\ &\quad + c_n \sinh(n+1)\alpha + d_n \sinh(n-1)\alpha, \end{aligned} \tag{2.9}$$

The integration constants B, K, A_n, B_n, C_n, D_n, a_n, b_n, c_n, d_n are given in the Appendix A1.

The components of the corresponding displacement vector are given by Jeffery (1921)

$$\begin{aligned} 2\mu u_\alpha &= (\cosh\alpha - \cos\beta)\left[\frac{\kappa-1}{2}\frac{\partial}{\partial\alpha}\left(\frac{h_\chi}{\cosh\alpha - \cos\beta}\right) - \frac{\kappa+1}{4}\frac{\partial}{\partial\beta}\left(\frac{h_Q}{\cosh\alpha - \cos\beta}\right)\right], \\ 2\mu u_\beta &= (\cosh\alpha - \cos\beta)\left[\frac{\kappa-1}{2}\frac{\partial}{\partial\beta}\left(\frac{h_\chi}{\cosh\alpha - \cos\beta}\right) + \frac{\kappa+1}{4}\frac{\partial}{\partial\alpha}\left(\frac{h_Q}{\cosh\alpha - \cos\beta}\right)\right], \end{aligned} \tag{2.10}$$

where $\kappa = 3\text{–}4\,\nu$ or $\kappa = (3-\nu)/(1+\nu)$ for plane strain or plane stress state, respectively, and

$$h_Q = \frac{2\tau_{12}^\infty(\cosh\alpha + \sinh^2\alpha - \cos\beta) - (\sigma_{11}^\infty - \sigma_{22}^\infty)\sin\beta\sinh\alpha}{\cosh\alpha - \cos\beta} + \left[2B\beta - 4K\tan^{-1}\left(\tanh\frac{\alpha}{2}\ \cot\frac{\beta}{2}\right)\right](\cosh\alpha - \cos\beta)$$

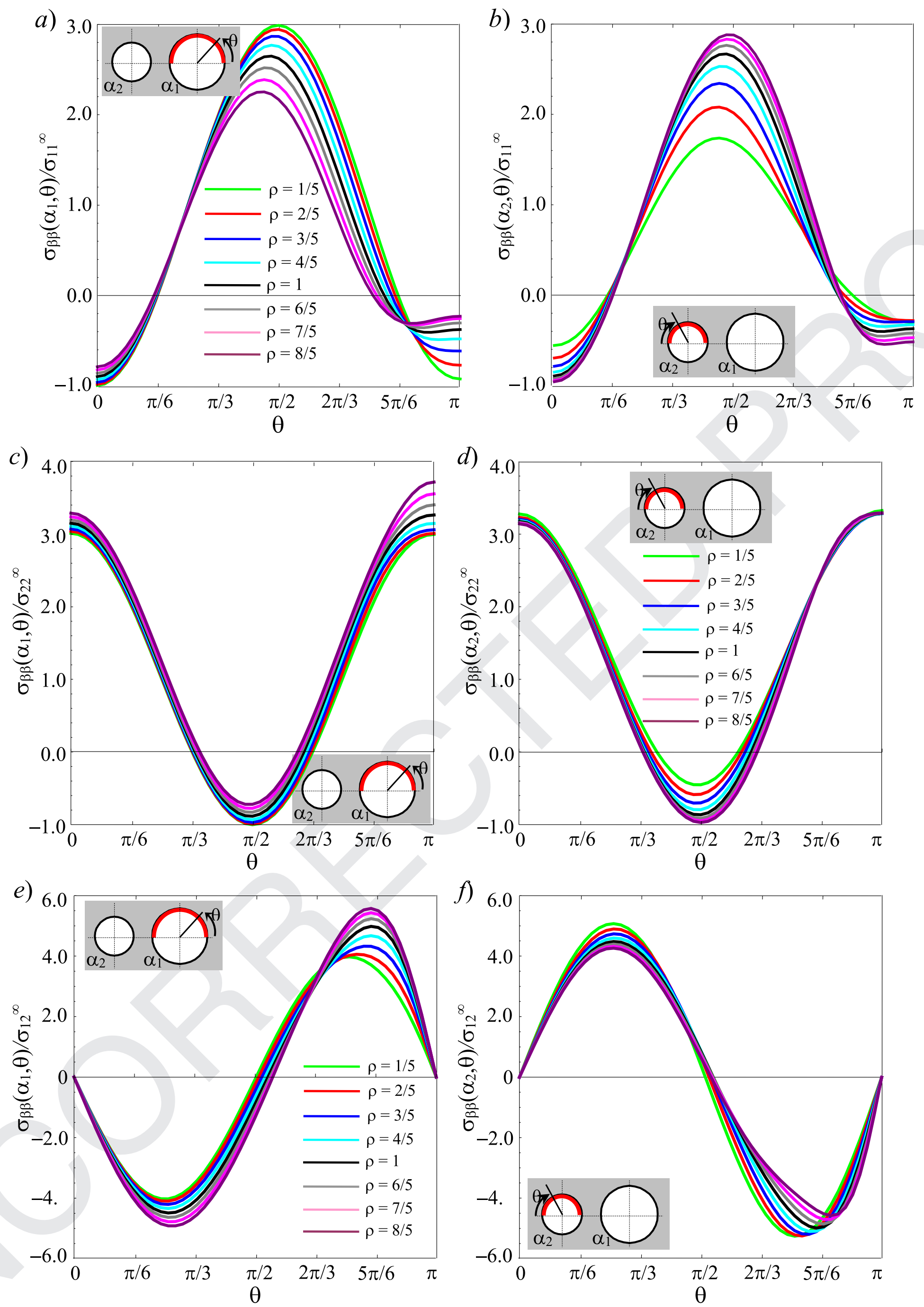

Fig. 8. Dimensionless hoop stress $\sigma_{\beta\beta}$ along the contour of the hole (a) with $\alpha = \alpha_1$ and (b) with $\alpha = \alpha_2$ for some values of ρ and $\gamma = 1$.

$$
\begin{aligned}
&+2(A_1 \sinh 2\alpha + C_1 \cosh 2\alpha)\sin\beta \\
&-2(a_1 \sinh 2\alpha + c_1 \cosh 2\alpha)\cos\beta \\
&+2\sum_{n=2}^{\infty}\{[A_n \sinh\,(n+1)\alpha + B_n \sinh(n-1)\alpha \\
&+C_n \cosh\,(n+1)\alpha + D_n \cosh\,(n-1)\alpha]\sin n\beta + \\
&-[a_n \sinh(n+1)\alpha + b_n \sinh\,(n-1)\alpha \\
&+\,c_n \cosh(n+1)\alpha\, + d_n \cosh(n-1)\alpha]\cos n\beta\}. \qquad (2.11)
\end{aligned}
$$

Figs. 5–7 show distribution of the dimensionless stress fields in a plate subjected to a remote stresses σ_{11}^{∞}, σ_{22}^{∞} and σ_{12}^{∞}, respectively. Fig. 8 illustrates distribution of the dimensionless hoop stress along the contours of the pores for some values of $\rho \equiv r_2/r_1$, $\gamma \equiv \delta/r_1 = 1$. Fig. 9 provides the same information for different values of γ and $\rho = 2$.

3. Two overlapped circular holes

The modeling of two overlapping circles differs considerably from the case discussed in Section 2: the circular contours represent two curves of constant β ($0 \le \beta_1 < \pi, -\pi \le \beta_2 < 0$) for $\alpha \in (-\infty, \infty)$ (Fig. 8). In this case, Fourier transforms have to be applied instead of the Fourier series (see, for example, Ling, 1947; 1948b; Dutt, 1960). The geometry of the problem is completely defined by three independent parameters, e.g. coordinates

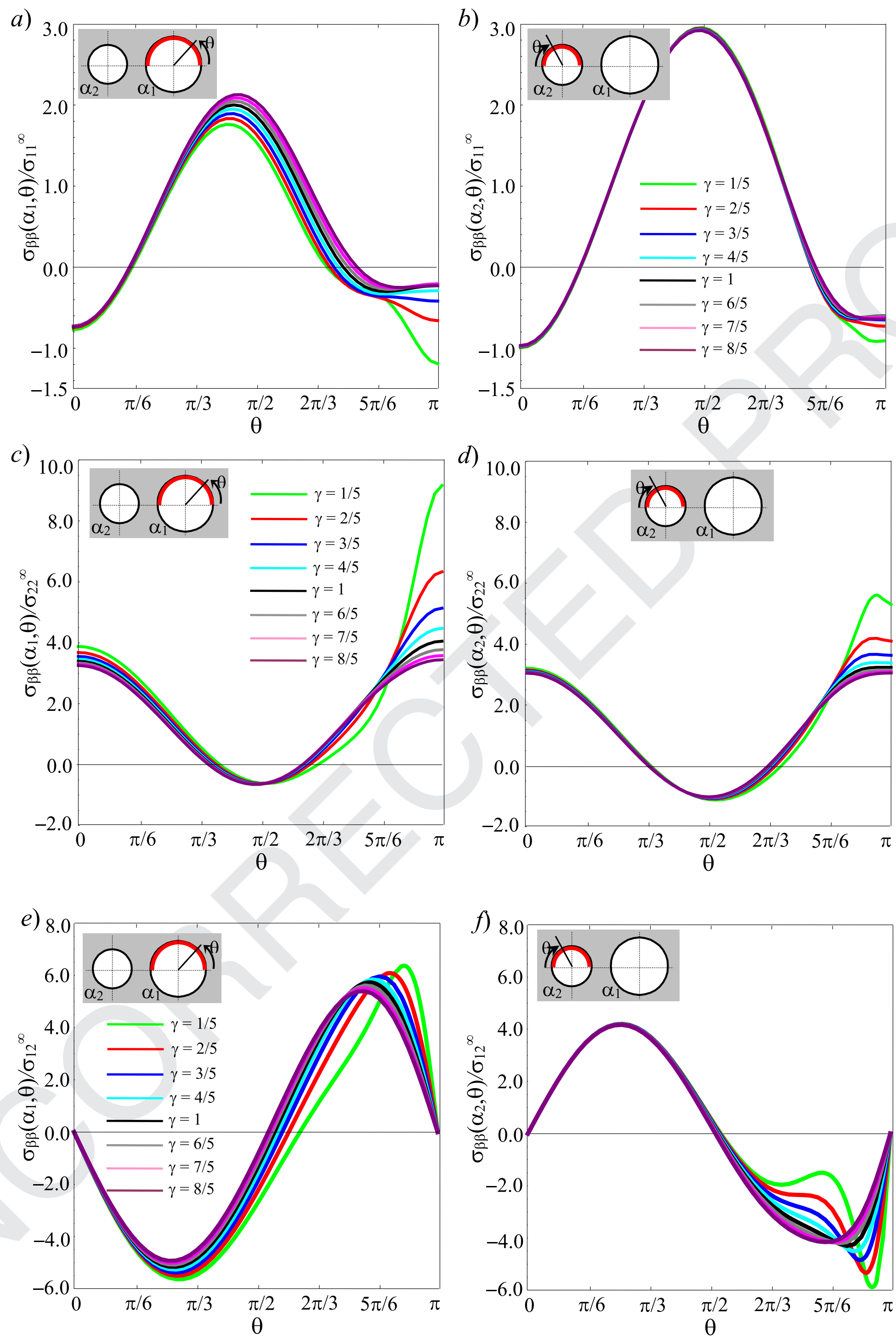

Fig. 9. Dimensionless hoop stress $\sigma_{\beta\beta}$ along the contour of the hole (a) with $\alpha = \alpha_1$ and (b) with $\alpha = \alpha_2$ for some values of γ and $\rho = 2$.

y_{c1}, y_{c2} of the centers of two circles and the focal distance a. Then, $\beta_1 = \arctan a/y_{c1}$, $\beta_2 = \arctan a/y_{c2}$, $r_1 = a/\sin|\beta_1|$, $r_2 = a/\sin|\beta_2|$, and the area included in the contour reads $A = {r_1}^2\,(\pi - \beta_1) + {r_2}^2\,(\pi + \beta_2) + a^2\,(\cot\beta_1 - \cot\beta_2)$. In contrast to the case of 2 separate holes, here the ligament δ turns out to be a negative quantity defined as $\delta = y_{c1} - r_1 - (y_{c2} + r_2)$.

The form of the fundamental stress function is the same as in (2.7), whereas the auxiliary stress functions are taken as follows:

$$h_\chi^{(1)} = \int_0^\infty F(s,\beta)\cos s\alpha + G(s,\beta)\sin s\alpha ds,$$

$$h_\chi^{(2)} = (\cosh\alpha - \cos\beta)\left\{K\log\frac{\cosh\alpha - \cos\beta}{\cosh\alpha + \cos\beta}\right\}, \tag{3.1}$$

where

$$\begin{aligned} F(s,\beta) &= f_F(s)\sin\beta\sinh s\beta + k_F(s)\cos\beta\cosh s\beta \\ &\quad + g_F(s)\sin\beta\cosh s\beta + h_F(s)\cos\beta\sinh s\beta; \\ G(s,\beta) &= f_G(s)\sin\beta\cosh s\beta + k_G(s)\cos\beta\sinh s\beta \\ &\quad + g_G(s)\sin\beta\sinh s\beta + h_G(s)\cos\beta\cosh s\beta. \end{aligned} \tag{3.2}$$

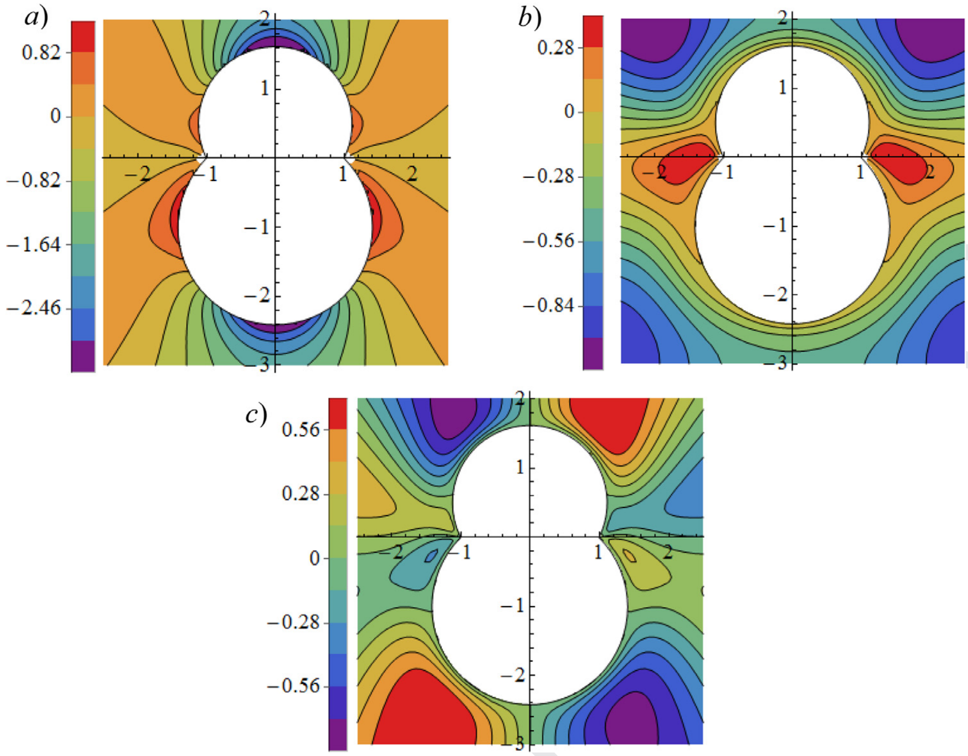

Fig. 10. Distribution of the dimensionless stress fields (a) $\sigma_{\alpha\alpha}/\sigma^{\infty}{}_{11}$; (b) $\sigma_{\beta\beta}/\sigma^{\infty}{}_{11}$; (c) $\sigma_{\alpha\beta}/\sigma^{\infty}{}_{11}$ in a plate subjected to a remote stress in the x_1 direction for $\kappa_1 = 1/2$ and $\kappa_2 = -1$.

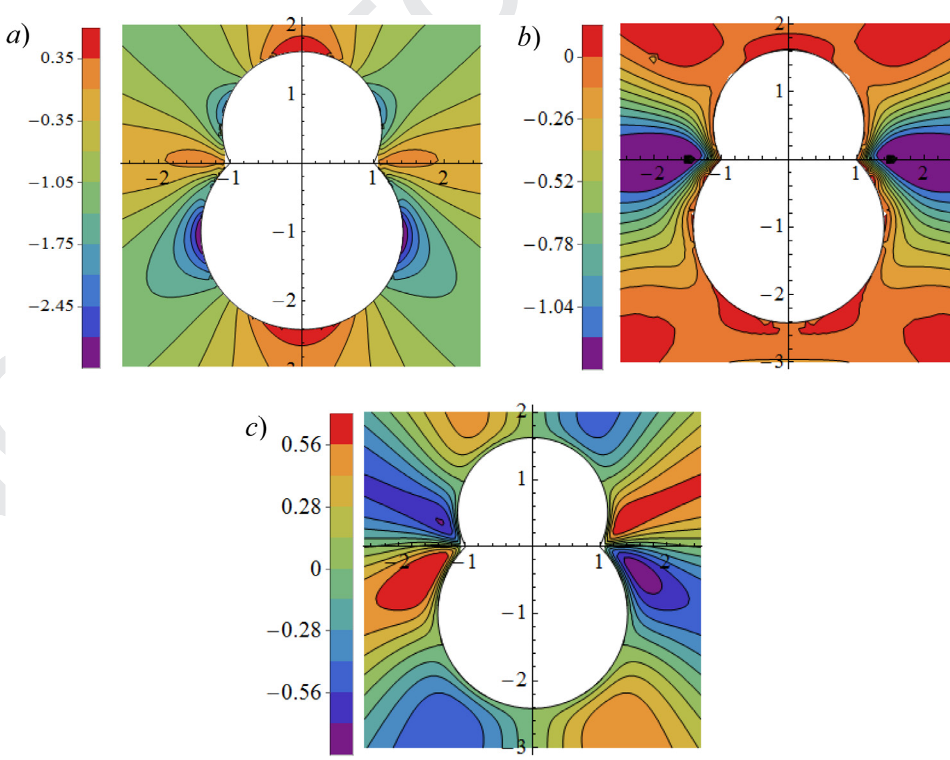

Fig. 11. Distribution of the dimensionless stress fields (a) $\sigma_{\alpha\alpha}/\sigma^{\infty}{}_{22}$; (b) $\sigma_{\beta\beta}/\sigma^{\infty}{}_{22}$; (c) $\sigma_{\alpha\beta}/\sigma^{\infty}{}_{22}$ in a plate subjected to a remote stress in the x_2 direction for $\kappa_1 = 1/2$ and $\kappa_2 = -1$.

Note also that a symmetric layout is retrieved if $\beta_2 = -\beta_1$: In such a case one has $g_F(s) = g_G(s) = h_F(s) = h_G(s) = 0$ (see Ling (1948b) for a plate with symmetric overlapped holes subjected to normal loadings and Karunes (1953) for the shear loading). For remotely applied shear loading it is $h_\chi(^2) = 0$.

The fundamental stress function (2.7) can be rewritten, after some algebra, in the following form:

$$h_\chi^{(0)} = \frac{(\Delta\sigma^\infty \sin^2\beta - 2\sigma_{12}^\infty \sin\beta \sinh\alpha)}{2(\cosh\alpha - \cos\beta)} + \sigma_{22}^\infty \cos\beta, \tag{3.3}$$

where $\Delta\sigma^\infty = (\sigma^\infty{}_{11} - \sigma^\infty{}_{22})$.

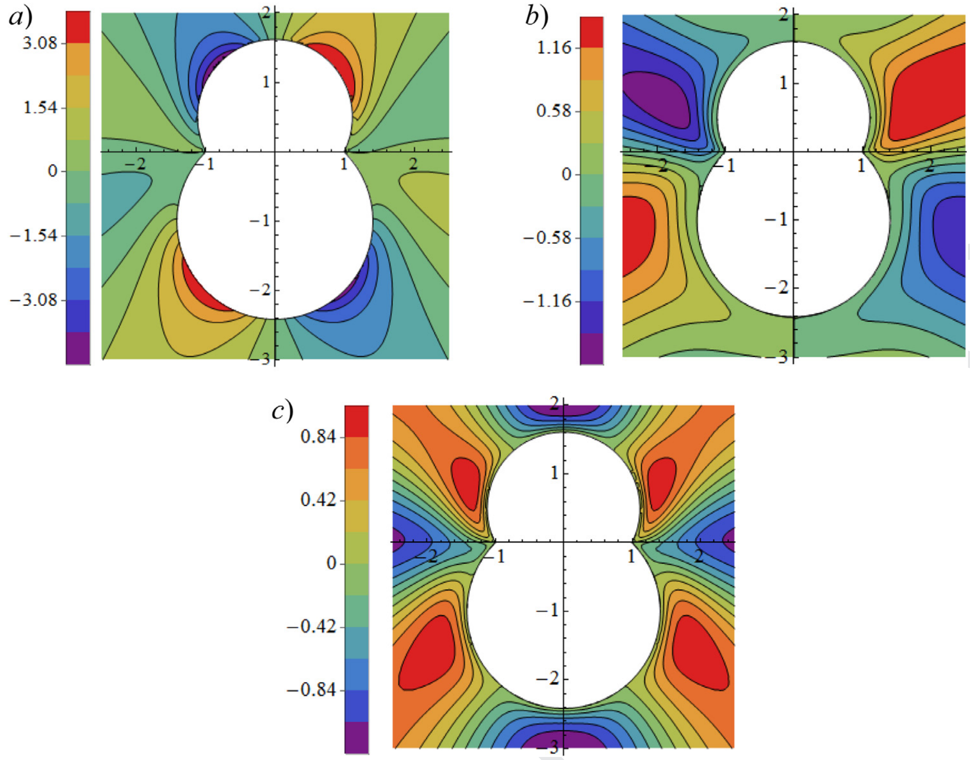

Fig. 12. Distribution of the dimensionless stress fields (a) $\sigma_{\alpha\alpha}/\sigma^{\infty}{}_{12}$; (b) $\sigma_{\beta\beta}/\sigma^{\infty}{}_{12}$; (c) $\sigma_{\alpha\beta}/\sigma^{\infty}{}_{12}$ in a plate subjected to a remote shear stress in the x_1x_2 plane for $\kappa_1 = 1/2$ and $\kappa_2 = -1$.

The traction-free boundary conditions at the hole are

$$\sigma_\beta = 0, \quad \tau_{\alpha\beta} = 0, \quad \text{for } \beta = \beta_1, \beta_2;$$
$$h_\chi{}^{(1)}(\alpha,\beta) + h_\chi{}^{(2)}(\alpha,\beta) = 0 \quad \text{for } \alpha, \beta \to 0. \tag{3.4}$$

The first two conditions can be reformulated for the auxiliary stress functions $h_\chi(^1)(\alpha,\beta)$ and $h_\chi(^2)(\alpha,\beta)$ as

$$\frac{\partial^2 h_\chi}{\partial\beta\,\partial\alpha} = 0, \text{ for } \beta = \beta_1, \beta_2. \tag{3.5}$$

and

$$\left[(\cosh\alpha - \cos\beta)\frac{\partial^2}{\partial\alpha^2} - \sinh\alpha\frac{\partial}{\partial\alpha} - \sin\beta\frac{\partial}{\partial\beta} + \cos\beta\right] h_\chi = 0, \text{ for } \beta = \beta_1, \beta_2. \tag{3.6}$$

The last of the conditions (3.4) yields

$$\int_0^\infty k_F(s)ds = 0. \tag{3.7}$$

Taking the derivative of expression (3.6) with respect to α and using (3.5) one can write

$$\frac{\partial}{\partial\alpha}\left[1 - \frac{\partial^2}{\partial\alpha^2}\right]h_\chi = 0, \text{ for } \beta = \beta_1, \beta_2, \tag{3.8}$$

and in turn, integration of (3.8) with respect to α gives

$$\left[1 - \frac{\partial^2}{\partial\alpha^2}\right]h_\chi + C_i = 0, \text{ for } \beta = \beta_i (i = 1, 2). \tag{3.9}$$

Expressions (3.5) and (3.9) can now be used to find unknown functions $f_F(s)$, $f_G(s)$, $k_F(s)$, $k_G(s)$, $g_F(s)$ and $h_F(s)$. Constant K follows from condition (3.7) for normal loading.

Condition (3.6) gives (for $\beta = \beta_1, \beta_2$).

$$\int_0^\infty F'(s,\beta)\sin s\alpha\, ds = \Delta\sigma^\infty \frac{(1 - \cos\beta\cosh\alpha)\sin\beta\sinh\alpha}{(\cosh\alpha - \cos\beta)^3} + B_0\sinh\alpha + K\frac{\sin 2\beta\,\sinh 2\alpha}{(\cosh\alpha + \cos\beta)^2(\cosh\alpha - \cos\beta)};$$
$$\int_0^\infty sG'(s,\beta)\cos s\alpha\, ds = -\sigma_{12}^\infty\frac{(3 - 4\cos\beta\cosh\alpha + \cos 2\beta\cosh 2\alpha)}{2(\cosh\alpha - \cos\beta)^3}, \tag{3.10}$$

where the apex denotes derivative with respect to coordinate β whereas from condition (3.9) one has

$$\int_0^\infty (1+s^2)F(s,\beta)\cos s\alpha\, ds = K\cos\beta\,\ln\frac{\cosh\alpha - \cos\beta}{\cosh\alpha + \cos\beta} + 2K\cos\beta + 2K\frac{\cos^2\beta}{\cosh\alpha + \cos\beta} - K\frac{\sin^2 2\beta}{(\cosh\alpha - \cos\beta)(\cos\alpha + \cos\beta)^2}$$
$$- \frac{\sigma_{11}^\infty}{2}\sin^2\beta\left(\frac{1}{\cosh\alpha - \cos\beta} + \frac{\cosh\alpha}{(\cosh\alpha - \cos\beta)^2} + - \frac{2\sinh^2\alpha}{(\cosh\alpha - \cos\beta)^3}\right) - \frac{\sigma_{22}^\infty}{2}\left(-\frac{2\cosh^2\alpha + \sinh^2\alpha}{(\cosh\alpha - \cos\beta)} + \frac{5\cosh\alpha\sinh^2\alpha}{(\cosh\alpha - \cos\beta)^2} - \frac{2\sinh^4\alpha}{(\cosh\alpha - \cos\beta)^3}\right) - C_i;$$
$$\int_0^\infty (1+s^2)G(s,\beta)\sin s\alpha ds = +\sigma_{12}^\infty\frac{3\cosh\alpha\sinh\alpha\sin\beta}{(\cosh\alpha - \cos\beta)^2} - \sigma_{12}^\infty\frac{2\sin\beta\sinh^3\alpha}{(\cosh\alpha - \cos\beta)^3} - \tilde{C}_i; \tag{3.11}$$

Eq. $(3.11)_{1,2}$ for $\alpha \to \infty$ yield

$$C_i = \left[2K - \sigma_{22}^\infty + B_0\beta\right]\cos\beta, \quad \tilde{C}_i = \sigma_{12}^\infty\sin\beta, \quad \text{for } \beta = \beta_i (i = 1, 2) \quad . \tag{3.12}$$

Thus, from Eqs. (3.10) and (3.11), taking into account results (3.12) one has for $\beta = \beta_i$ $(i = 1, 2)$

$$
\begin{aligned}
F'(s,\beta_i) &= \frac{2a\Delta\sigma^\infty}{s\pi}\int_0^\infty \sin s\alpha \frac{(1-\cos\beta\cosh\alpha)\sin\beta\sinh\alpha}{(\cosh\alpha-\cos\beta)^3}d\alpha \\
&+\frac{2K}{s\pi}\int_0^\infty \sin s\alpha\frac{\sin 2\beta\sinh 2\alpha}{(\cosh\alpha+\cos\beta)^2(\cosh\alpha-\cos\beta)}d\alpha; \\
G'(s,\beta_i) &= -\sigma_{12}^\infty\frac{2}{s\pi} \\
&\int_0^\infty \frac{(3-4\cos\beta\cosh\alpha+\cos 2\beta\cosh 2\alpha)}{2(\cosh\alpha-\cos\beta)^3}\cos s\alpha d\alpha
\end{aligned}
\tag{3.13}
$$

and

$$
\begin{aligned}
F(s,\beta_i) &= \frac{2K}{(1+s^2)\pi}\cos\beta\int_0^\infty \cos s\alpha\ln\frac{\cosh\alpha-\cos\beta}{\cosh\alpha+\cos\beta}d\alpha \\
&+\frac{4K}{(1+s^2)\pi}\cos^2\beta\int_0^\infty\frac{\cos s\alpha}{\cosh\alpha+\cos\beta}d\alpha+ \\
&-\frac{2K}{(1+s^2)\pi}\sin^2 2\beta\int_0^\infty\frac{\cos s\alpha}{(\cosh\alpha-\cos\beta)(\cos\alpha+\cos\beta)^2}d\alpha+ \\
&+a\frac{\Delta\sigma^\infty}{(1+s^2)\pi}\sin^2\beta\int_0^\infty\cos s\alpha\left(\frac{3\cos\beta}{(\cos\alpha-\cos\beta)^2}\right. \\
&\left.-\frac{2\sin^2\beta}{(\cos\alpha-\cos\beta)^3}\right)d\alpha; \\
G(s,\beta_i) &= -\frac{2\sigma_{12}^\infty}{(1+s^2)\pi}\sin\beta\int_0^\infty\sin s\alpha d\alpha \\
&+\frac{6\sigma_{12}^\infty}{(1+s^2)\pi}\sin\beta\int_0^\infty\frac{\cosh\alpha\sinh\alpha\sin s\alpha}{(\cosh\alpha-\cos\beta)^2}d\alpha+ \\
&-\frac{4\sigma_{12}^\infty}{(1+s^2)\pi}\sin\beta\int_0^\infty\frac{\sinh^3\alpha\sin s\alpha}{(\cosh\alpha-\cos\beta)^3}d\alpha.
\end{aligned}
\tag{3.14}
$$

Note that, through the results reported in Appendix A2, all the Fourier transforms involved in the Eqs. (3.13) and (3.14) can be evaluated in closed form, thus allowing to find the analytic expressions of functions $F(s, \beta)$, $G(s, \beta)$ and their derivatives:

$$
\begin{aligned}
F(s,\beta) &= -2K\cos\beta\frac{\sinh s(\frac{\pi}{2}-|\beta|)}{s(1+s^2)\cosh\frac{s\pi}{2}}+4K\cos^2\beta\frac{\sinh s\beta}{(1+s^2)\sinh s\pi\sin\beta} \\
&-a\Delta\sigma^\infty\sin^2\beta\csc|\beta|\mathrm{csch}s\pi\sinh s(\pi-|\beta|)+ \\
&-K\sin^2 2\beta\frac{\sec\beta\sinh s(\pi-|\beta|)-2s\cosh s\beta\csc|\beta|-(-2\cot\beta\csc\beta+\sec|\beta|)\sinh s|\beta|}{2(1+s^2)\sin|\beta|\cos\beta\sinh s\pi}; \\
G(s,\beta) &= 2\sigma_{12}^\infty\frac{\pi s(1+s^2)\cosh s(\pi-|\beta|)\mathrm{csch}(\pi s)-1}{s\pi(1+s^2)}\sin|\beta|; \\
F'(s,\beta) &= 4K\sin 2\beta\frac{s\cos\beta\sinh s|\beta|+\sinh\frac{s\pi}{2}\sinh s(\frac{\pi}{2}-|\beta|)\sin|\beta|}{s\sin|2\beta|\sinh s\pi} \\
&+a\Delta\sigma^\infty\sin\beta\frac{s(s\cosh s(\pi-|\beta|)-\sinh s(\pi-|\beta|)\cot|\beta|}{s\sinh s\pi}; \\
G'(s,\beta) &= 2\sigma_{12}^\infty\mathrm{csch}s\pi[\cos\beta\cosh s(\pi-|\beta|)-s\sin|\beta|\sinh s(\pi-|\beta|)].
\end{aligned}
\tag{3.15}
$$

System (3.15) imposed for $\beta = \beta_i$ $(i = 1, 2)$ allows assessing functions $f_F(s)$, $f_G(s)$, $k_F(s)$, $k_G(s)$, $g_F(s)$, $g_G(s)$, $h_F(s)$ and $h_G(s)$ and, in turn, the stress and displacement fields according to Eqs. (2.4) and (2.10), respectively. For the case of two equal overlapping holes $\beta_1 = -\beta_2$ the expressions of $f_F(s)$, $k_F(s)$ reported in Ling (1948b) for normal loadings and $f_G(s)$, $k_G(s)$ reported in Karunes (1953) for shear loadings are exactly retrieved (actually, a misprint occurred in expression $(16)_1$ of F_n reported in Karunes (1954), in which the square in "n^2" must be removed). Figs. 10–12 illustrate distribution of the dimensionless stress fields in a plate subjected to a remote stresses σ_{11}^∞, σ_{22}^∞ and σ_{12}^∞, respectively.

4. Evaluation of the compliance contribution tensor

Compliance contribution tensors have been first introduced by Horii and Nemat-Nasser (1983) for pores of ellipsoidal shape (explicit formulas connecting compliance contribution tensor and Eshelby tensor for an ellipsoidal pore are given in the appendix of the mentioned paper). Components of this tensor for various two-dimensional pores were given by Kachanov et al. (1994) and for ellipsoidal inhomogeneities – by Sevostianov and Kachanov (1999). This tensor connects the extra strain due to the presence of the inhomogeneity under given remotely applied stresses. Indeed, if we consider a representative volume element V containing an isolated inhomogeneity of volume V_1, the average, over representative volume V strain can be represented as a sum

$$\boldsymbol{\varepsilon} = \boldsymbol{S}^0 : \boldsymbol{\sigma}^0 + \Delta\boldsymbol{\varepsilon} \tag{4.1}$$

where $\mathbf{S}^0$ is the compliance tensor of the matrix and $\boldsymbol{\sigma}^0$ represents the uniform boundary conditions (tractions on ∂V have the form $\mathbf{t}|_{\partial V} = \boldsymbol{\sigma}^0 \cdot \mathbf{n}$ where $\boldsymbol{\sigma}^0$ is a constant tensor); $\boldsymbol{\sigma}^0$ can be viewed as far-field ("remotely applied") stress. The material is assumed to be linear elastic; hence the extra strain due to the inhomogeneity $\Delta\,\boldsymbol{\varepsilon}$ is a linear function of $\boldsymbol{\sigma}^0$:

$$\Delta\boldsymbol{\varepsilon} = \frac{V_1}{V}\boldsymbol{H} : \sigma^0 \tag{4.2}$$

where $\mathbf{H}$ is a fourth-rank compliance contribution tensor of the inhomogeneity. If the inhomogeneity is a pore, the extra overall strain due its presence is given by the well-known expression in terms of an integral over the pore boundary (Hill, 1963):

$$\Delta\varepsilon = \frac{1}{2V}\int_{\partial V}(\boldsymbol{un}+\boldsymbol{nu})dS \tag{4.3}$$

Thus, Neumann boundary value problem has to be solved in order to find the compliance contribution tensor of a pore.

4.1. *Two separate circular inhomogeneities (symmetric with respect to x_1 axis)*

The components of the unit vector and the infinitesimal arc length on the contour of the two circles with $\alpha = const$ are:

$$
\begin{aligned}
n_1 &= -\frac{\cosh\alpha_i\cos\beta-1}{\cosh\alpha_i-\cos\beta}sign(\alpha_i), \quad n_2 = -\frac{\sinh|\alpha_i|\sin\beta}{\cosh\alpha_i-\cos\beta} \\
ds &= r_i d\theta = \frac{a\,sign(\alpha_i)}{\cosh\alpha_i-\cos\beta}d\beta, \quad i = 1,2
\end{aligned}
\tag{4.4}
$$

where θ is the polar angle measured from x_1 axis as shown in Fig. 13(a). In the Cartesian coordinate system (x_1, x_2), the components of the unit vector, the displacement field and the infinitesimal arc length on the contour of the two separate circles with

Please cite this article as: L. Lanzoni, E. Radi and I. Sevostianov, Effect of pair coalescence of circular pores on the overall elastic properties, International Journal of Solids and Structures, https://doi.org/10.1016/j.ijsolstr.2019.05.012

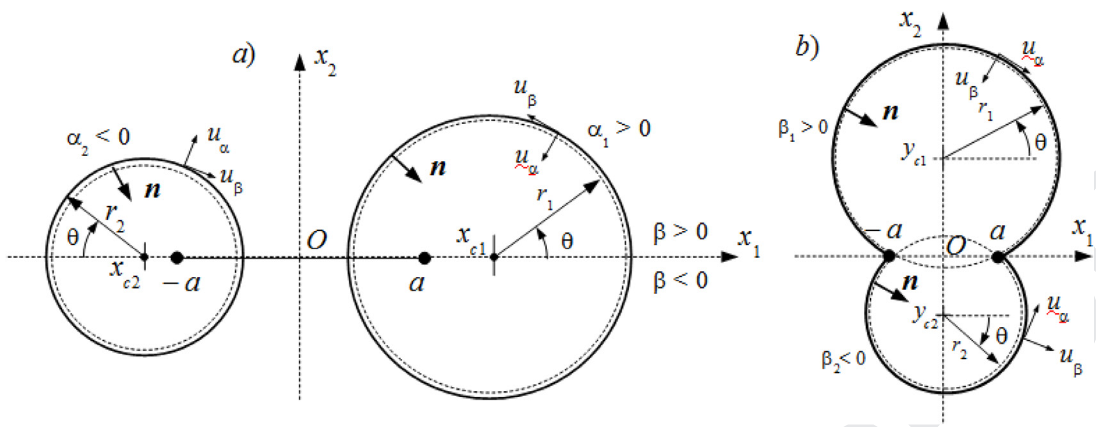

Fig. 13. Sketch of the polar coordinate systems used to perform the circular integrals involved in expression (4.2) for the components of the extra overall strain.

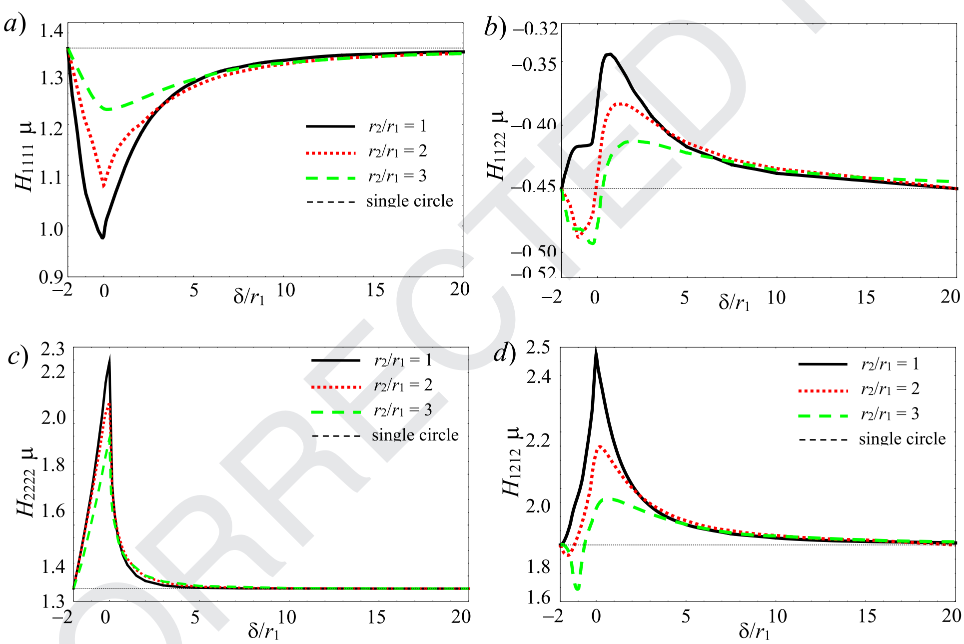

Fig. 14. Normalized components of the cavity compliance tensor (a) $H_{1111}\ \mu$; (b) $H_{1122}\ \mu$; (c) $H_{2222}\ \mu$; (d) $H_{1212}\ \mu$ for some values of ρ. Reference is made to plane strain condition.

α = const are

$$u_1 = -u_\alpha \cos\theta - u_\beta \sin\theta; \qquad u_2 = -u_\alpha \sin\theta + u_\beta \cos\theta; \quad (4.5)$$

with

$$\cos\theta = \frac{\cosh\alpha_i \cos\beta - 1}{\cosh\alpha_i - \cos\beta}\mathrm{sign}(\alpha_i);\ \sin\theta = \frac{\sinh|\alpha_i|\sin\beta}{\cosh\alpha_i - \cos\beta};$$
$$ds = r_i d\theta = \frac{a\,\mathrm{sign}(\alpha_i)}{\cosh\alpha_i - \cos\beta}d\beta, \quad (4.6)$$

and

$$\begin{aligned}&\text{for}\ \alpha = \alpha_1 > 0: \quad n_1 = -\cos\theta; \quad n_2 = -\sin\theta;\\ &\text{for}\ \alpha = \alpha_1 < 0: \quad n_1 = \cos\theta; \quad n_2 = -\sin\theta.\end{aligned} \quad (4.7)$$

Now, using results of the Section 2 and formulas (4.3) compliance contribution tensor can be calculated for two separate pores (the integral has to be evaluated numerically).

4.2. Overlapped circles symmetric with respect to x_2 axis

The component of the unit vector and the infinitesimal arc length on the contour at $\beta = const$ are

$$n_1 = -\frac{\sinh\alpha\ \sin\beta_i}{\cosh\alpha - \cos\beta_i}sign(\beta_i);\ n_2 = -\frac{1 - \cosh\alpha\ \cos\beta_i}{\cosh\alpha - \cos\beta_i}sign(\beta_i)$$
$$ds = r_i d\theta = -\frac{a\ sign(\beta_i)}{\cosh\alpha - \cos\beta_i}d\alpha, \quad i = 1, 2 \quad (4.8)$$

For the overlapping holes (Fig. 13(b)), one finds

$$u_1 = u_\alpha \sin\theta - u_\beta \cos\theta;\ u_2 = -u_\alpha \cos\theta - u_\beta \sin\theta; \quad (4.9)$$

$$\begin{aligned}&\text{for}\ \beta = \beta_1 > 0: \quad n_1 = -\cos\theta; \quad n_2 = -\sin\theta;\\ &\text{for}\ \beta = \beta_2 < 0: \quad n_1 = -\cos\theta; \quad n_2 = \sin\theta;\end{aligned} \quad (4.10)$$

$$\cos\theta = \frac{\sinh\alpha\ \sin\beta_i}{\cosh\alpha - \cos\beta_i}; \quad \sin\theta = \frac{1 - \cosh\alpha\ \cos\beta_i}{\cosh\alpha - \cos\beta_i},$$

Please cite this article as: L. Lanzoni, E. Radi and I. Sevostianov, Effect of pair coalescence of circular pores on the overall elastic properties, International Journal of Solids and Structures, https://doi.org/10.1016/j.ijsolstr.2019.05.012

$$ds = r_i\, d\theta = -\frac{a\, sign(\beta_i)}{\cosh\alpha - \cos\beta_i} d\alpha. \tag{4.11}$$

Taking into account that the area of the pore cross-section $A_i = r_i^2(\pi - |\beta_i + (\sin|2\beta_1|)/2|)$, one can use results of Section 3 and formula (4.3) to evaluate the compliance contribution tensor.

Fig. 14 illustrates the dimensionless components of the compliance contribution tensor in dependence on δ/r_1 for different values of r_2/r_1.

5. Concluding remarks

In this paper, we calculated compliance contribution tensor of two separate or intersecting circular pores. For this goal, we first considered two holes and solved Neumann boundary value problem in two-steps: (1) assessment of the fundamental displacement field related to a remotely applied uniform stress in a homogeneous body and (2) fulfillment of the boundary conditions in the problem with pores by adding an extra-term to the fundamental field. This solution was used to construct the compliance contribution tensor of the combination of two circular pores by calculating proper contour integrals. Plots for H_{1111} and H_{2222} (Fig. 14(a) and (c)) generally reproduce the curves for two corresponding components of the resistivity contribution tensor (Lanzoni et al., 2018). At the same time, components H_{1122} and H_{1212} behave differently and may show non-monotonic not only near $\delta/r_1 = 1$ (point where the circles touch each other), but also when $\delta/r_1 > 1$ or $\delta/r_1 < 1$ (see Fig. 14(b) and (d)). This is in agreement with expressions for cross-property connections for a material with ellipsoidal/elliptical pores and inhomogeneities derived by Sevostianov and Kachanov (2002, 2008). In particular, for a two-dimensional elliptical hole

$$\boldsymbol{H} = \frac{1}{E_0}\left[\frac{(2a_2+a_1)}{a_1}\boldsymbol{e}_1\boldsymbol{e}_1\boldsymbol{e}_1\boldsymbol{e}_1 + \frac{(2a_1+a_2)}{a_2}\boldsymbol{e}_2\boldsymbol{e}_2\boldsymbol{e}_2\boldsymbol{e}_2 + \frac{(a_1+a_2)^2}{2a_1a_2}(\boldsymbol{e}_1\boldsymbol{e}_2+\boldsymbol{e}_2\boldsymbol{e}_1)(\boldsymbol{e}_1\boldsymbol{e}_2+\boldsymbol{e}_2\boldsymbol{e}_1) - (\boldsymbol{e}_1\boldsymbol{e}_1\boldsymbol{e}_2\boldsymbol{e}_2+\boldsymbol{e}_2\boldsymbol{e}_2\boldsymbol{e}_1\boldsymbol{e}_1)\right] \tag{5.1}$$

$$\boldsymbol{R} = \frac{1}{k_0}\left(\frac{a_1+a_2}{a_1}\boldsymbol{e}_1\boldsymbol{e}_1 + \frac{a_1+a_2}{a_2}\boldsymbol{e}_2\boldsymbol{e}_2\right) \tag{5.2}$$

So that

$$E_0H_{1111} = k_0R_{11}\left[1+\frac{1}{k_0R_{22}}\right]; \quad E_0H_{2222} = k_0R_{22}\left[1+\frac{1}{k_0R_{11}}\right];$$
$$E_0H_{1212} = \frac{1}{k_0R_{11}} + \frac{1}{k_0R_{22}}; \quad E_0H_{1122} = \frac{(R_{11}+R_{22})^2}{R_{11}R_{22}} \tag{5.3}$$

Components R_{11} and R_{22} that behave oppositely (one increases when another decreases) enter expressions for H_{1122} and H_{1212} in concurrent manner, so that their combined effect may be quite complex.

The case $\delta/r_1 = -2$, $r/r_1 = 1$ corresponds to an isolated circular inhomogeneity. In this case, the well-known result for the compliance contribution tensor of a circular hole (see Horii and Nemat-Nasser, 1983) is recovered. The compliance contribution tensor constitutes the basic building block for calculation of the overall elastic properties of a material containing parallel cylindrical holes with the cross-sections shown in Fig. 2 (see Kachanov and Sevostianov, 2018)

Acknowledgments

Financial support from the Italian Ministry of Education, University and Research (MIUR) in the framework of the Project PRIN 2017 *Modelling of constitutive laws for traditional and innovative building materials* (code 2017HFPKZY) is gratefully acknowledged. IS and ER acknowledge financial support of Indam-GNFM "Gruppo Nazionale per la Fisica Matematica".

Appendices

A1. Integration constants used in Section 2

$$A_1 = \frac{1}{D}\cosh(\alpha_1+\alpha_2)\{2f(\alpha_1)\sinh^2\alpha_2 - 2f(\alpha_2)\sinh^2\alpha_1 + [g(\alpha_1)-g(\alpha_2)]\tanh(\alpha_1+\alpha_2)\}, \tag{A1.1}$$

$$B_1 = \frac{1}{D}\cosh(\alpha_1-\alpha_2)\{2f(\alpha_2)\sinh^2\alpha_1 - 2f(\alpha_1)\sinh^2\alpha_2 - [g(\alpha_1)+g(\alpha_2)]tanh(\alpha_1-\alpha_2) + g(\alpha_2)sinh2\alpha_1 - g(\alpha_1)sinh2\alpha_2\} \tag{A1.2}$$

$$C_1 = \frac{1}{D}\cosh(\alpha_1+\alpha_2)\{g(\alpha_2)-g(\alpha_1) + [f(\alpha_1)-f(\alpha_2)]tanh(\alpha_1+\alpha_2) + f(\alpha_2)sinh2\alpha_1 - f(\alpha_1)sinh2\alpha_2\} \tag{A1.3}$$

$$B = B = \frac{2}{D}\cosh(\alpha_1-\alpha_2)\{[f(\alpha_1)+f(\alpha_2)]\tanh(\alpha_1-\alpha_2) + g(\alpha_2)-g(\alpha_1)\}, \tag{A1.4}$$

where:

$$f(\alpha) = 2K\,e^{-|\alpha|}\sinh\ \alpha - (\sigma_{22}^\infty - \sigma_{11}^\infty)e^{-2|\alpha|}sign\,\alpha,$$
$$g(\alpha) = \cosh 2\alpha - e^{-|\alpha|}(\sigma_{11}^\infty\cosh\alpha + \sigma_{22}^\infty\sinh|\alpha|), \tag{A1.5}$$

$$D = 2\sinh(\alpha_1-\alpha_2)(\sinh^2\alpha_1 + \sinh^2\alpha_2) \tag{A1.6}$$

$$a_1 = \tau_{12}^\infty\frac{e^{-2|\alpha_1|}\cosh 2\alpha_2 - e^{-2|\alpha_2|}\cosh 2\alpha_1}{\sinh 2(\alpha_1-\alpha_2)}, \tag{A1.7}$$

$$c_1\tau_{12}^\infty\frac{e^{-2|\alpha_1|}\sinh 2\alpha_2 + e^{-2|\alpha_2|}\sinh 2\alpha_1}{\sinh 2(\alpha_1-\alpha_2)}. \tag{A1.8}$$

$$A_n = \frac{1}{H_n}\{P_n(\alpha_1,\alpha_2)\Phi_n(\alpha_1) + P_n(\alpha_2,\alpha_1)\Phi_n(\alpha_2) + Q_n(\alpha_1,\alpha_2)\Phi_n*(\alpha_1) + Q_n(\alpha_2,\alpha_1)\Phi_n*(\alpha_2) \tag{A1.9}$$

$$B_n = \frac{1}{H_n}\{P_{-n}(\alpha_1,\alpha_2)\Phi_n(\alpha_1) + P_{-n}(\alpha_2,\alpha_1)\Phi_n(\alpha_2) + Q_{-n}(\alpha_1,\alpha_2)\Phi_n*(\alpha_1) + Q_{-n}(\alpha_2,\alpha_1)\Phi_n*(\alpha_2)\} \tag{A1.10}$$

$$C_n = -\frac{1}{H_n}\{U_n(\alpha_1,\alpha_2)\Phi_n(\alpha_1) + U_n(\alpha_2,\alpha_1)\Phi_n(\alpha_2) + [V_n(\alpha_1,\alpha_2) + cosh(2n\alpha_2 - (n-1)\alpha_1)]\Phi_n*(\alpha_1) + V_n(\alpha_2,\alpha_1)\Phi_n*(\alpha_2)\} \tag{A1.10A}$$

$$D_n = \frac{1}{H_n}\{U_{-n}(\alpha_1,\alpha_2)\Phi_n(\alpha_1) + U_{-n}(\alpha_2,\alpha_1)\Phi_n(\alpha_2) + V_{-n}(\alpha_1,\alpha_2)\Phi_n*(\alpha_1) + V_{-n}(\alpha_2,\alpha_1)\Phi_n*(\alpha_2)\} \tag{A1.11}$$

$$a_n = \frac{1}{H_n}\{P_n(\alpha_1,\alpha_2)\Psi_n(\alpha_1) + P_n(\alpha_2,\alpha_1)\Psi_n(\alpha_2) + Q_n(\alpha_1,\alpha_2)\Psi_n*(\alpha_1) + Q_n(\alpha_2,\alpha_1)\Psi_n*(\alpha_2)\} \tag{A1.12}$$

Please cite this article as: L. Lanzoni, E. Radi and I. Sevostianov, Effect of pair coalescence of circular pores on the overall elastic properties, International Journal of Solids and Structures, https://doi.org/10.1016/j.ijsolstr.2019.05.012

$$b_n = \frac{1}{H_n}\{P_{-n}(\alpha_1,\alpha_2)\Psi_n(\alpha_1) + P_{-n}(\alpha_2,\alpha_1)\Psi_n(\alpha_2) + Q_{-n}(\alpha_1,\alpha_2)\Psi_n*(\alpha_1) + Q_{-n}(\alpha_2,\alpha_1)\Psi_n*(\alpha_2)\} \tag{A1.13}$$

$$c_n = -\frac{1}{H_n}\{U_n(\alpha_1,\alpha_2)\Psi_n(\alpha_1) + U_n(\alpha_2,\alpha_1)\Psi_n(\alpha_2) + [V_n(\alpha_1,\alpha_2) + cosh(2n\alpha_2 - (n-1)\alpha_1)]\Psi_n*(\alpha_1) + V_n(\alpha_2,\alpha_1)\Psi_n*(\alpha_2)\} \tag{A1.14}$$

$$d_n = \frac{1}{H_n}\{U_{-n}(\alpha_1,\alpha_2)\Psi_n(\alpha_1) + U_{-n}(\alpha_2,\alpha_1)\Psi_n(\alpha_2) + V_{-n}(\alpha_1,\alpha_2)\Psi_n*(\alpha_1) + V_{-n}(\alpha_2,\alpha_1)\Psi_n*(\alpha_2)\} \tag{A1.15}$$

for $n \geq 2$, where

$$P_n(\xi,\eta) = \frac{1}{n+1}(\sinh(\xi+n\eta)\,\sinh n(\xi-\eta) + n\,\sinh(\xi+n\xi)\,\sinh(\xi-\eta)), \tag{A1.16}$$

$$Q_n(\xi,\eta) = \cosh\,(\xi+n\eta)\mathrm{sigh}\,n(\xi-\eta) - n\,\cosh(\eta+n\xi)\,\sinh(\xi-\eta), \tag{A1.17}$$

$$U_n(\xi,\eta) = \frac{1}{n+1}[\cosh(\xi+n\eta)\,\sinh n(\xi-\eta) + n\,\cosh(\eta+n\xi)\,\sinh(\xi-\eta)], \tag{A1.18}$$

$$V_n(\xi,\,\eta) = \sinh(\xi+n\eta)\,\sinh\,n(\xi-\eta) - n\,\sinh(\eta+n\xi)\,\sinh(\xi-\eta), \tag{A1.19}$$

$$H_n = 2n\{\sinh^2[n(\alpha_1-\alpha_2)] - n^2\sinh^2(\alpha_1-\alpha_2)\}. \tag{A1.20}$$

$$\Phi_n*(\alpha) = 2K\,e^{-n|\alpha|}\sinh\,\alpha - (\sigma_{22}^{\infty} - \sigma_{11}^{\infty})n\,g_n(\alpha)\mathrm{sign}\,\alpha, \tag{A1.21}$$

$$\Phi_n(\alpha) = -e^{-n|\alpha|}[2\,K\,(\cosh\,\alpha + n\,\mathrm{sign}|\alpha|) + (\sigma_{22}^{\infty} - \sigma_{11}^{\infty})\,n\,(n^2-1)\,\sinh|\sigma_{22}^{\infty}|] \tag{A1.22}$$

$$\Psi_n*(\alpha) = 2\,n\,g_n(\alpha) \tag{A1.23}$$

$$\Psi_n(\alpha) = 2\,\tau_{12}^{\infty}\,n\,(n^2-1)\,e^{-n|\alpha|}\sinh\alpha. \tag{A1.24}$$

Finally, the constant K follows from the condition

$$\sum_{n=1}^{\infty}(A_n + B_n) = 0. \tag{A1.25}$$

after the introduction of the constants A_n and B_n, for $n \geq 1$.

A2. Useful Fourier transforms

The following definite integrals have been used to find expressions (3.13) and (3.14):

$$\int_0^{\infty}\frac{(1-\cos\beta\cosh\alpha)\sinh\alpha}{(\cosh\alpha-\cos\beta)^3}\sin s\alpha ds = \frac{\pi}{2}s\frac{(s\cosh s(\pi-|\beta|) - \sinh s(\pi-|\beta|)\cot|\beta|)}{\sinh s\pi}; \tag{A2.1}$$

$$\int_0^{\infty}\frac{\sinh 2\alpha}{(\cosh\alpha-\cos\beta)(\cosh\alpha+\cos\beta)^2}\sin s\alpha ds = 2\pi\frac{s\sinh s|\beta|\cos\beta + \sinh\frac{s\pi}{2}\sinh s\left(\frac{\pi}{2}-|\beta|\right)\sin|\beta|}{\sinh s\pi\,\sin 2|\beta|}; \tag{A2.2}$$

$$\int_0^{\infty}\frac{\cos s\alpha}{(\cosh\alpha-\cos\beta_{\mathrm{i}})}d\alpha = \pi\frac{\sinh s(\pi-|\beta_{\mathrm{i}}|)}{\sinh s\pi\,\sin|\beta_{\mathrm{i}}|}; \tag{A2.3}$$

$$\int_0^{\infty}\frac{\cos s\alpha}{(\cosh\alpha+\cos\beta_{\mathrm{i}})}d\alpha = \pi\frac{\sinh s|\beta_{\mathrm{i}}|}{\sinh s\pi\,\sin|\beta_{\mathrm{i}}|}; \tag{A2.4}$$

$$\int_0^{\infty}\frac{\cos s\alpha}{(\cosh\alpha+\cos\beta_{\mathrm{i}})^2}d\alpha = \pi\frac{s\cosh\beta_{\mathrm{i}} - \cot|\beta_{\mathrm{i}}|\sinh s|\beta_{\mathrm{i}}|}{\sinh s\pi\sin^2|\beta_{\mathrm{i}}|}; \tag{A2.5}$$

$$\int_0^{\infty}\log\left(\frac{\cosh\alpha-\cos\beta_{\mathrm{i}}}{\cosh\alpha+\cos\beta_{\mathrm{i}}}\right)\cos s\alpha d\alpha = -\pi\frac{\sinh s\left(\frac{\pi}{2}-|\beta_{\mathrm{i}}|\right)}{s\cosh\left(s\frac{\pi}{2}\right)}; \tag{A2.6}$$

$$\int_0^{\infty}\frac{\cos s\alpha}{(\cosh\alpha-\cos\beta_{\mathrm{i}})^2}d\alpha = \pi\frac{s\cosh s(\pi-|\beta_{\mathrm{i}}|) + \cot|\beta_{\mathrm{i}}|\sinh s(\pi-|\beta_{\mathrm{i}}|)}{\sin^2\beta_{\mathrm{i}}\sinh s\pi}; \tag{A2.7}$$

$$\int_0^{\infty}\frac{\cos s\alpha}{(\cosh\alpha-\cos\beta_{\mathrm{i}})^3}d\alpha = \pi\frac{3s\cosh s(\pi-|\beta_{\mathrm{i}}|)\cot|\beta_{\mathrm{i}}| + (s^2-2+3\csc^2\beta_{\mathrm{i}})\sinh s(\pi-|\beta_{\mathrm{i}}|)}{\sin^3|\beta_{\mathrm{i}}|\sinh s\pi}; \tag{A2.8}$$

$$\int_0^{\infty}\frac{\cos s\alpha}{(\cosh\alpha-\cos\beta)(\cosh\alpha+\cos\beta)^2}d\alpha = = \pi\frac{sec|\beta|\sinh s(\pi-|\beta|)\cos\beta - 2s\cosh s\beta\csc\beta - (sec|\beta| - 2\cot|\beta|\csc\beta)\sinh s|\beta|}{4\sin|\beta|\cos\beta\sinh s\pi}; \tag{A2.9}$$

$$\int_0^{\infty}\frac{\cosh\alpha}{(\cosh\alpha-\cos\beta_{\mathrm{i}})}\cos(s\alpha)d\alpha = \pi\frac{\sinh s(\pi-|\beta_{\mathrm{i}}|)\cos\beta_{\mathrm{i}}}{\sinh s\pi\,\sin|\beta_{\mathrm{i}}|}; \tag{A2.10}$$

$$\int_0^{\infty}\frac{\cosh\alpha}{(\cosh\alpha-\cos\beta_{\mathrm{i}})^2}\cos(s\alpha)d\alpha = \pi\frac{s\cosh s(\pi-|\beta_{\mathrm{i}}|)\cot|\beta_{\mathrm{i}}| + \csc^2|\beta_{\mathrm{i}}|\sinh s(\pi-|\beta_{\mathrm{i}}|)}{\sinh s\pi\,\sin|\beta_{\mathrm{i}}|}; \tag{A2.11}$$

$$\int_0^{\infty}\frac{\sinh\alpha}{(\cosh\alpha-\cos\beta_{\mathrm{i}})^2}\sin(s\alpha)d\alpha = s\pi\frac{\sinh s\pi\cosh s\beta_{\mathrm{i}} - \cosh s\pi\sinh|s\beta_{\mathrm{i}}|}{\sinh s\pi\,\sin|\beta_{\mathrm{i}}|}; \tag{A2.12}$$

$$\int_0^\infty \frac{\cos s\alpha}{(\cosh\alpha - \cos\beta_\mathrm{i})^2}\mathrm{d}\alpha = \pi\,\frac{\cosh s\beta_\mathrm{i}(s\coth s\pi + \cot|\beta_\mathrm{i}|) - \sinh s|\beta_\mathrm{i}|(s + \cot|\beta_\mathrm{i}|\coth s\pi)}{\sin^2\beta_\mathrm{i}}; \tag{A2.13}$$

References

Drenchev, L., Sobczak, J., 2009. Gasars. A specific Class of Porous Materials. Motor Transport Institute, Krakow.
Dutt, S.B., 1960. On the stresses due to an overlapped circular hole on the neutral axis of a deep beam under constant bending moment. Appl. Sci. Res. 9, 457–462.
Ekneligoda, T.C., Zimmerman, R.W., 2006. Compressibility of two-dimensional pores having n-fold axes of symmetry. Proc. R. Soc. A 462, 1933–1947.
Ekneligoda, T.C., Zimmerman, R.W., 2008b. Boundary perturbation solution for nearly-circular holes and rigid inclusions in an infinite elastic medium. ASME J. Appl. Mech. 75 paper 011015-1.
Ekneligoda, T.C., Zimmerman, R.W., 2008a. Shear compliance of two-dimensional pores possessing N-fold axis of rotational symmetry. Proc. R. Soc. A 464, 759–775.
Hill, R., 1963. Elastic properties of reinforced solids: some theoretical principles. J.Mech.Phys.Solids 11, 357–372.
Horii, H., Nemat-Nasser, S., 1983. Overall moduli of solids with microcracks: load-induced anisotropy. J. Mech. Phys. Solids 31, 155–171.
Jasiuk, I., 1995. Cavities vis-a'-vis rigid inclusions: elastic moduli of materials with polygonal inclusions. Int. J. Solids Struct. 32, 407–422.
Jeffery, G.B., 1921. Plane stress and plane strain in bipolar co-ordinates. Philos. Trans. R. Soc. Lond. Ser. A 221, 265–293.
Kachanov, M., Sevostianov, I., 2018. Micromechanics of Materials, With Applications. Springer.
Kachanov, M., Tsukrov, I., Shafiro, B., 1994. Effective moduli of solids with cavities of various shapes. Appl. Mech. Rev. 47, S151–S174.
Karunes, B., 1953. On the concentration of stress round the edge of a hole bounded by two intersecting circles in a large plate. Indian J. Phys. 27, 208–212.
Lanzoni, L., Radi, E., Sevostianov, I., 2018. Effect of cylindrical fibers of irregular cross-section on the overall thermal conductivity of a composite. Int. J. Solids Struct. 138, 264–276.
Ling, C.-B., 1947. On the stresses in a notched plate under tension. J. Math. Phys. 26, 284–289.
Ling, C.B., 1948a. On the stresses in a plate containing two circular holes. J.f Appl. Phys. 19, 77–82.
Ling, C.B., 1948b. The stresses in a plate containing an overlapped circular hole. J. Appl. Phys. 19, 405–411.
Liu, X., Li, Y., Wang, J., He, Y., 2018. The pore growth process and pore coalescence process in Gasar copper. Mater. Character. 137, 231–243.
Radi, E., 2011. Path-independent integrals around two circular holes in an infinite plate under biaxial loading conditions. Int. J. Eng. Sci. 49, 893–914.
Sevostianov, I., Kachanov, M., 1999. Compliance tensors of ellipsoidal inclusions. Int. J. Fract. 96, L3–L7.
Shapovalov, V., 1994. Porous metals. MRS Bull. 19 (4), 24–28.
Shapovlov, V.I., 1998. Formation of ordered gas-solid structures via solidification in metal-hydrogen systems. Mater. Res. Soc. Symp. Proc. 521 (Symposium R), 281–290.
Shapovalov, V., Boyko, L., 2004. Gasar - anew class of porous materials. Adv. Eng. Mater. 6, 407–410.
Tsukrov, I., Novak, J., 2002. Effective elastic properties f solids with defects of irregular shape. Int. J. Solids Struct. 39, 1539–1555.
Tsukrov, I., Novak, J., 2004. Effective elastic properties of solids with two-dimensional inclusions of irregular shape. Int. J. Solids Struct. 41, 6905–6924.
Zimmerman, R.W., 1986. Compressibility of two-dimensional cavities of various shapes. J. Appl. Mech. 53, 500–504.

Please cite this article as: L. Lanzoni, E. Radi and I. Sevostianov, Effect of pair coalescence of circular pores on the overall elastic properties, International Journal of Solids and Structures, https://doi.org/10.1016/j.ijsolstr.2019.05.012